Multi-sensor-based method for early detection of bacterial wilt of tobacco

Xiangfeng Zeng[1,2#], Yanyan Li[3#], Jie Li[2], Zhen Pu[1,2], Lu Zheng[2], Peng Song[1,2*]

(1. *National Key Laboratory of Crop Genetic Improvement, Huazhong Agricultural University, Wuhan 430070, China*;
2. *College of Science & Technology, Huazhong Agricultural University, Wuhan 430070, China*;
3. *Tobacco Research Institute of Hubei Province, Wuhan 430030, China*)

Abstract: Tobacco is a significant economic crop in China, but it is susceptible to various diseases and insect pests, including the highly contagious tobacco bacterial wilt disease. The disease can cause severe damage with no possibility of eradication once it occurs. In this study, we collected hyperspectral and visible light data of tobacco seedlings at different stages of the disease development and compared the detection performance of the two methods. We proposed the XGBoost ensemble learning algorithm to construct a detection model for tobacco bacterial wilt disease based on the characteristic bands selected from hyperspectral data. The model achieved an accuracy of 92.20% for all samples. Additionally, an improved model Tobacco-AT was designed based on visible light images, introducing the attention mechanism with focusing function into the current popular target detection model framework, achieved high accuracy on tobacco bacterial wilt data set. Detection performance of the two methods was compared, and the results showed that the hyperspectral model had an accuracy of 69.57% on the first day after inoculation, while the accuracy of Tobacco-AT was only 54.66%. However, the accuracy of visible light based method (Tobacco-AT) was close to that of the hyperspectral based method at 85.00% and 86.36% on the third day, which demonstrates the potential of visible light technology for early detection and the possibility of being a low-cost solution.

Keywords: Tobacco bacterial wilt detection; hyperspectral imaging; deep learning; plant disease early detection; classification algorithm

DOI: 10.33440/j.ijpaa.20230601.219

Citation: Zeng X F, Li Y Y, Li J, Pu Z, Zheng L and Song P. Multi-sensor-based method for early detection of bacterial wilt of tobacco. Int J Precis Agric Aviat, 2023; 6(1): 33–43.

1 Introduction

Tobacco is a crucial economic crop in China, contributing significantly to the country's national income. Tobacco bacterial wilt is one of the main diseases of tobacco in tropical and subtropical regions, with a local incidence rate of more than 80% and often mixed with tobacco black shank disease. Severe cases can cause the entire field of tobacco to wither and die, making it a significant threat to tobacco farmers' livelihoods[1,2]. Furthermore, the disease is highly contagious, and once it occurs, it can quickly spread throughout the entire field, even resulting in crop failure. Therefore, it is very important to obtain timely and accurate information on the status and spatial distribution of tobacco bacterial wilt in order to reduce secondary infection through biological control and even early removal of susceptible plants[3]. However, traditional tobacco bacterial wilt detection methods, such as field investigation, manual identification and chemical detection, are often time-consuming, inefficient, expensive and even destructive[4]. Therefore, non-contact, non-destructive, advanced and automated detection methods are favored by researchers and farmers. They can provide accurate disease information in near real time[5], which is helpful to achieve the purpose of early detection of bacterial wilt and cultivation of tobacco varieties with high resistance to bacterial wilt.

After being infected by the pathogen resulting tobacco bacterial wilt, the leaf mesophyll cells undergo destruction, leading to a decrease in water content and causing the leaves to turn yellow and dry. This, in turn, leads to a decrease in chlorophyll content and the leaf area index. These changes affect the total amount of reflected or emitted radiation from tobacco leaves, providing the possibility for remote sensing technology to rapidly and extensively monitor the occurrence and development of bacterial wilt in tobacco. In the early stages of tobacco bacterial wilt disease, the leaves retain their green color, and the difference in color compared to healthy leaves is minimal. Therefore, the disease can only be discerned through the observation of leaf morphology, where infected leaves may exhibit slight wilting.

In recent years, crop phenotyping technologies have emerged as a crucial solution in agricultural research and crop breeding[6]. With the development of computer vision and artificial intelligence technology, crop disease diagnosis methods based on visible and near-infrared spectroscopy technology have gained widespread acceptance[7-9]. Zhang et al. summarized the application of hyperspectral methods in disease detection and commonly used data acquisition platforms[10]. Gu et al. achieved success in the early detection of tomato spotted wilt virus infection in tobacco using the hyperspectral imaging technique and machine learning algorithms[11]. Yusuf et al. showed that the wavelengths of 730 and 790 nm were most useful for distinguishing tobacco black shank[12]. Scholars also carried out early detection of tobacco diseases[13]. For instance, Zhu investigated the feasibility and potentiality of presymptomatic detection of tobacco disease using hyperspectral imaging, combined with the variable selection

Received date: 2023-11-15 **Accepted date:** 2023-12-15

Biographies: Xiangfeng Zeng, Postgraduate student, research interests: crop phenotyping, Email: 843040386@qq.com; **Yanyan Li**, PhD, research interests: tobacco disease, Email: yanyanli0025@126.com; Jie Li, Postgraduate student, research interests: tobacco disease prevention and control, Email: jieli0121@126.com; **Zhen Pu**, Postgraduate student, research interests: hyperspectral data processing, Email: 2214119388@qq.com; **Lu Zheng**, PhD, research interests: plant pathology, Email: luzheng@mail.hzau.edu.cn.

***Corresponding author: Peng Song,** PhD, research interests: crop phenotyping, Email: songp@mail.hzau.edu.cn.

[#] Xiangfeng Zeng and Yanyan Li are the co-first authors

method and machine-learning classifiers[14].

While near-infrared spectroscopy and hyperspectral imaging contains more information than visible light images, visible light images can be easily obtained through various ordinary electronic devices such as digital cameras and smartphones, making them more feasible for disease image recognition in the visible light range. With the improvement of computer image computing power, deep learning methods show great potential in target detection tasks. More and more scholars have also applied this technology to plant disease detection[15-18]. Kumar developed a deep learning model that can use convolutional neural networks to classify and detect diseases in tobacco plants[19]. Compared with traditional algorithms, deep learning algorithms perform better in accuracy. Sujatha compared the effect of traditional machine learning and deep learning, the disease classification accuracy (CA) is quite impressive as DL methods perform better than that of ML methods[19]. And the model has strong adaptability and achieved good results in detection of various plant diseases[8,20,21]. Complex scenes in the field have always been the difficulty in plant disease detection. To address the robustness and accuracy issues caused by complex image backgrounds, Zeng proposed a self-attention convolutional neural network (SACNN) to identify crop diseases by extracting the most effective features of crop diseases[22]. In the detection of crop bacterial wilt, many scholars have successfully carried out early detection, with high accuracy and simple way to obtain images[23].

This study focuses on dynamic detection of tobacco bacterial wilt disease at a daily scale using hyperspectral and visible light techniques. The dataset underwent rigorous processing and analysis to establish high-performance models, resulting in a systematic and rapid non-destructive phenotypic detection approach for tobacco bacterial wilt disease. Furthermore, a comprehensive comparison and analysis of the two methods were conducted, aiming to achieve enhanced accuracy, simplicity, and cost-effectiveness. The findings provide valuable insights into the characteristic bands of the disease and demonstrate the potential of object detection technology as a low-cost solution for early detection, which provides ample time for implementing common practices like early harvesting to minimize losses and isolating infected plants to prevent further spread.

2 Materials and methods

2.1 Experimental material and Phenotyping equipment

The experiment utilized Yunyan 87 variety, which was bred in the plant pathology laboratory of Huazhong Agricultural University in April 2022. Yunyan 87 is a flue-cured tobacco variety widely planted in China (more than 80% of the area), which was approved by the National Variety Approval Committee in December 2000. Yunyan 87 is a hybrid of Yunyan 2 as the female parent and K326 as the male parent. It is a stable variety with a smaller coefficient of variation than K326 and exhibits resistance to black shank and leaf spot, and moderately resistant to southern root knot nematode and tobacco bacterial wilt. The experimental materials mainly consisted of seedlings in the early growth stage and were planted on the high-throughput crop phenotype platform of Huazhong Agricultural University in May 2022. The plants were cultivated in an artificial climate box to ensure normal growth and then divided into susceptible plants and control plants (healthy plants) for further analysis, as shown in Figure 1. Our materials are provided by Hubei Academy of Tobacco Science, and permitted to use in this study, with which all experiments in accordance with the relevant provisions of China.

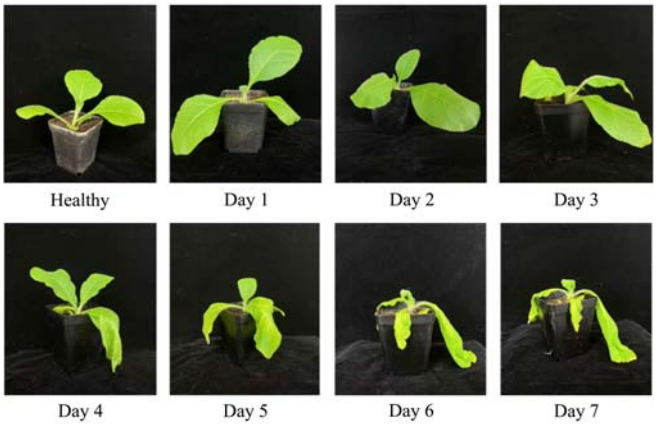

Figure 1 The changes of tobacco plants over time in the whole course of disease

To make the experimental data more uniform, we chose the plants with relatively consistent growth in the seedling pot, three batches of experiments were carried out. The first batch of materials was 28 plants, 8 plants were healthy plants and 20 plants were susceptible plants. The second batch of materials was 13 strains, 4 strains were healthy materials, 9 strains were susceptible materials, the third batch was 35 strains, 6 strains were healthy materials, and 29 strains were susceptible materials.

In this experiment, the intelligent crop information acquisition platform of Huazhong Agricultural University is used for data acquisition, which can realize the automatic and non-destructive acquisition of the trait parameters of greenhouse seedbed crops. The system is mainly composed of three-coordinate motion unit, image acquisition unit and control unit, as shown in Figure 2. The main structure of the platform is made of aluminum alloy, which is installed on the seedbed with a size of 7000 × 2000 × 1950 mm. The system uses a three-axis motion unit, driven by a stepper motor and an accurate motion control card (ECI2000, China Zmotion). The motion distance of each axis is 6100 mm for the X axis, 950 mm for the Y axis, and 500 mm for the Z axis. The image acquisition unit adopts an RGB camera (MARS-1230-23U3C, China Daheng) which is installed on the Y axis of the platform. The resolution of the camera is 4096 × 3000 pixels with a field of view of 530 mm × 388 mm on the canopy of the plant. The spectral range of the hyperspectral camera (FX10e, Finland) is 400~1000 nm. For the full width at half maximum is 5.5 nm, there are 224 spectral bands' data for all the samples[24].

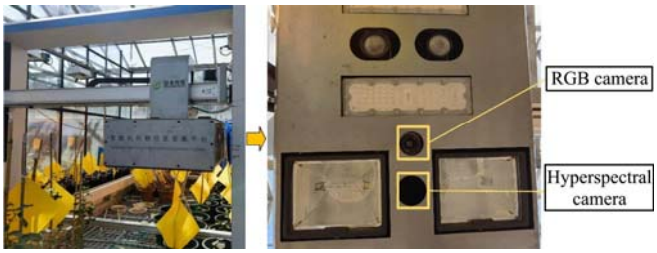

Figure 2 Intelligent crop phenotyping platform

2.2 Experimental processes

After the "four leaves and one heart" stage, tobacco plants were transplanted from the cultivation basin to small square basins measuring 5 cm × 5 cm × 7 cm. The medium used was a mixture of nutrient soil and vermiculite in a 3:1 ratio, appropriate water was supplemented to maintain humidity, and trace element reagents were added to ensure the normal growth of the plant. The plants were then cultivated in the greenhouse of the plant pathology

laboratory of Huazhong Agricultural University, with a temperature of 28°C and a daily illumination time of 16 hours. After reaching a height of approximately 10 cm, the plants were artificially inoculated with Ralstonia solanacearum using the pricking method, with a pathogen concentration of OD600=0.4. OD600 is an abbreviation for Optical Density at a wavelength of 600 nm. It is commonly used in spectrophotometry to estimate the concentration of bacteria or other cells in a liquid. By monitoring the rate of increase in OD600, the lag, log, and stationary phases of a bacterial culture can be identified. 1OD=log10(1/trans)[25]. After inoculation, the plants were transferred to the indoor phenotyping platform for data collection.

As can be seen from Figure 1, tobacco leaves show visible symptoms starting from the third day after inoculation with bacterial wilt. Therefore, we hope to conduct disease detection in the early stage of infection, which is within three days after infection. In this experiment, the plants were observed with 24-hour intervals. To ensure high-quality data acquisition, image captures were performed in the morning when the plants were in their normal state. The duration of visible light image acquisition last for 2-3 hours each time. Therefore, we conduct visible light data collection between 8-11 am each day. The hyperspectral image is collected at night. We use a halogen lamp as a fixed light source. Whiteboard correction and blackboard correction are performed before each shooting. Figure 3 shows the scenes of tobacco plants cultivation and data acquisition. Leaves that exhibit symptoms in the later stages of infection are marked as infected leaves during continuous observation, regardless of whether they exhibit symptoms in the early stages.

The dataset comprises infected and healthy plant images with dimensions of 3000×2000 pixels, each image in the dataset contains multiple tobacco plants, with each plant having multiple leaves. In total, there are 735 infected leaf samples as well as 459 healthy leaf samples available for analysis.

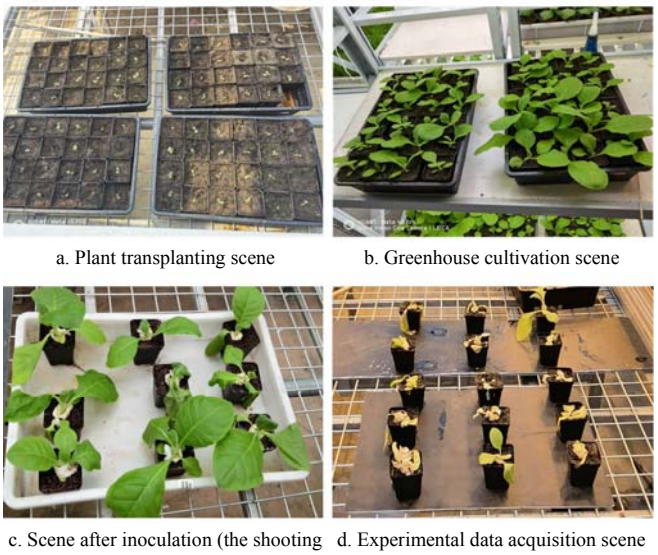

a. Plant transplanting scene b. Greenhouse cultivation scene

c. Scene after inoculation (the shooting time is the third day of inoculation) d. Experimental data acquisition scene

Figure 3 The whole process of experimental material growth and data acquisition

2.3 Data processing

Students with knowledge of tobacco bacterial wilt are responsible for judging and dividing the plants after inoculation. Label the data set according to the results of their division. Data was collected and classified into hyperspectral data and visible light data (RGB image), which have different formats. As a result, two separate processing methods were employed, taking into account the unique characteristics of each data set. A range of methods were carefully selected and modeled, and a unified evaluation method was utilized to assess their effectiveness. The data processing flow chart for this study is presented in Figure 4.

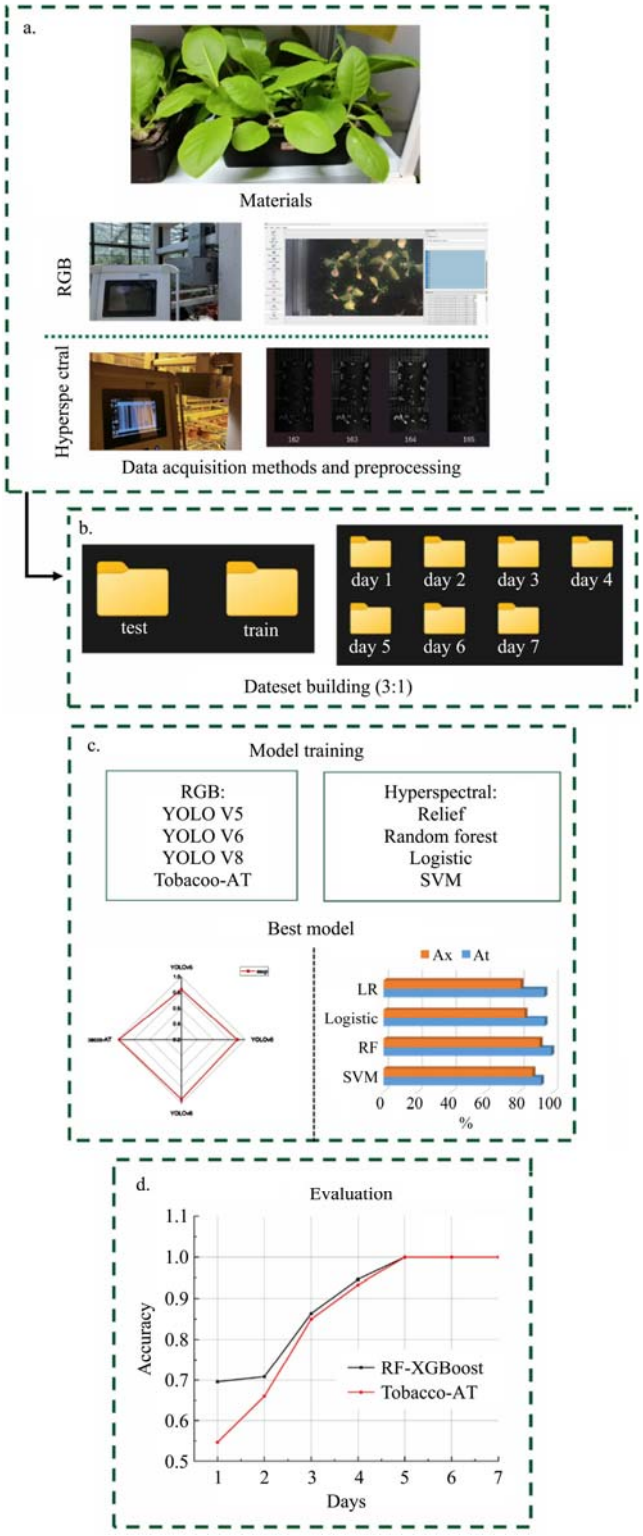

Figure 4 Processes of data processing

2.3.1 Hyperspectral data processing

1) ROI extraction

Based on the hyperspectral data collected, this study focuses on the segmentation method of individual tobacco plants using LabVIEW software, aimed at accurately extracting the single plant tobacco area. The data is then combined with this method to

extract the total reflectance and average reflectance of tobacco ROI (region of interest) area. The first step involves reading the captured data and extracting the original images of all 224 bands. In the second step, two bands (No.29 and No.156) with clear background and ROI region information are selected for threshold segmentation, followed by denoising operation using the small region removal module to obtain a binary image. Finally, the obtained binary image is mapped onto the original image as a mask to obtain ROI region in the hyperspectral data (Figure 5). The data of each leaf was then segmented manually.

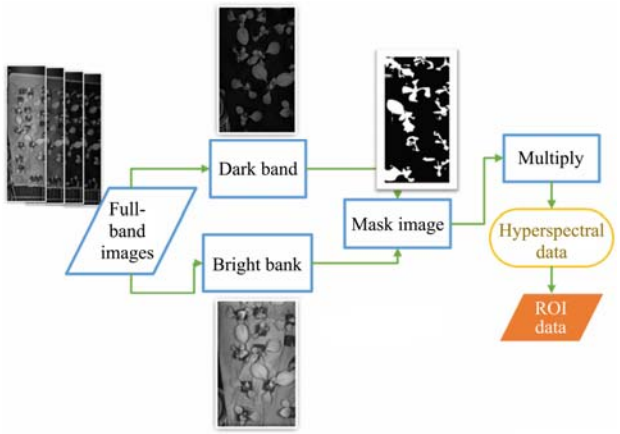

Figure 5 ROI extraction process

2) Data pre-processing

In the preceding steps, only the total reflectance data of each band in each leaf region was extracted. As environmental factors during plant growth are variable and individual differences among plants, the average reflectance can better demonstrate the difference between susceptible and healthy plants. So, we calculated the average reflectivity based on area information and visualized the hyperspectral average reflectance curve of tobacco plants. Each curve represented the spectral data of all bands of a single plant (Figure 6a).

Prior to constructing the model, preprocessing can make the data set features more apparent, facilitating easier learning by the classifier. Building on the average reflectivity data, we further processed the data, including first-order derivative, second-order derivative, and Log function, before combining it with the classical machine learning model. To identify the most interpretable method and prepare for subsequent feature band identification, we conducted pre-experiments on the dataset using three methods: random forest (RF), logistic regression (logistics), and support vector machine (SVM). The divided hyperspectral dataset for tobacco bacterial wilt was used for testing.

The preprocessed spectral data set is subjected to classification based on labels, resulting in two sets of data representing the average spectral data of infected and healthy plants. Visualization of the data in Figure 6b illustrates a discernible difference between the two sets, although some bands overlap. To model this distinction, three high-performance classifiers - XGBoost, LightGBM, and SVM - are combined with the preprocessed data, and their classification effects are compared. The classifier with high precision and recall rate is then selected to establish the optimal model.

3) Feature bands selection

Due to the high information content and dimensionality of hyperspectral data, appropriate methods for dimensionality reduction and feature band selection are necessary. We use random forest, logistic regression, stepwise regression and lasso regression to reduce the dimensionality of the data and then use it with the SVM classifier to evaluate the classification results. The results of the study, as depicted in Figure 7, demonstrated that the random forest algorithm exhibited superior performance.

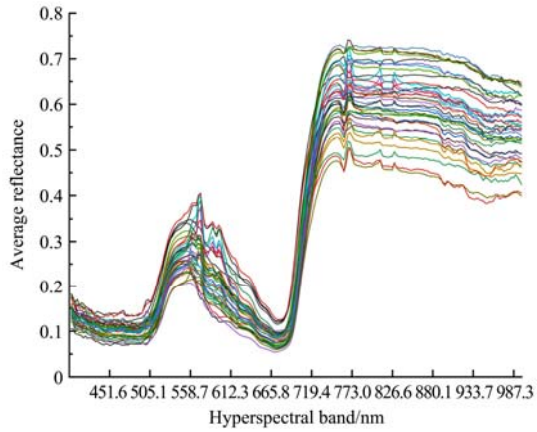

a. Original spectrum (using the third experimental data display), and figure

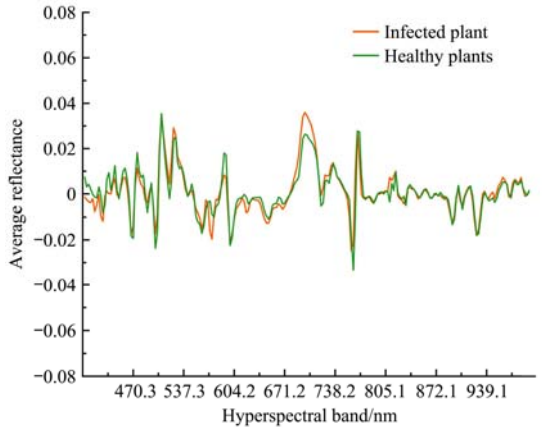

b. Average curve of the first derivative of the average reflectance of healthy plants and infected plants

Figure 6 Spectral data visualization

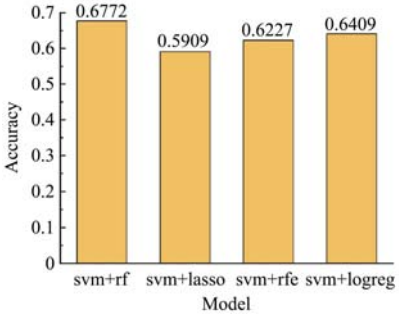

Figure 7 Feature screening accuracy

Nevertheless, this algorithm suffers from overfitting and poor robustness. To address these concerns, the Extreme Gradient Boosting (XGBoost) ensemble learning algorithm was introduced, which utilizes gradient boosting tree algorithms to determine feature importance[26]. The algorithm computes feature importance based on the number of splits or split gains for each feature in all trees. These values are then utilized to estimate the relevance of each feature to the classifier and, consequently, for feature selection purposes.

XGBoost is a machine learning algorithm based on gradient boosting decision tree, which is widely used in classification and regression tasks. The main advantages of XGBoost including: (1) Strong scalability, able to handle large-scale data. (2) Robust, can automatically handle missing values and outliers. (3) High

accuracy can optimize the objective function and regularization term to improve the model fitting degree. (4) Good interpretability and can give the order of feature importance. The objective function of XGBoost consists of two parts, the loss function and the regularization term. The loss function measures the degree of model fitting, and the regularization term prevents overfitting of the model. The loss function uses the weighted version of gradient boosting decision tree algorithm, and the regularization term is a linear combination of L1 and L2 regularization terms.

Equation (1) presents the objective function of XGBoost:

$$Obj^{(t)} = \sum_{i=1}^{n} L(y_i, \widehat{y_i^{(t-1)}} + f_t(x_i)) + \Omega(f_t) \tag{1}$$

where, $L(y_i, \widehat{y_i^{(t-1)}} + f_t(x_i))$ is the loss function; y_i is the true value of sample i; $\widehat{y_i^{(t-1)}}$ is the predicted value of the model after t–1 iterations; $f_t(x_i)$ is the splitting node in iteration t, and $\Omega(f_t)$ is the regularization term.

After sorting the eigenvalues, the partition points are traversed, and the optimal splitting income is taken as the splitting income of the feature. The feature with the optimal splitting income is selected as the division feature of the current node, and the binary division is performed according to its optimal division point to obtain the left and right subtrees. The formula for calculating the split score is shown in Equation (2):

$$gain = \frac{1}{2}\left[\frac{G_L^2}{H_L+\lambda} + \frac{G_R^2}{H_R+\lambda} - \frac{(G_L+G_R)^2}{H_L+H_R+\lambda}\right] - \gamma \tag{2}$$

where, G_L and G_R are the gradient sums of the left and right child nodes; H_L and H_R are the Hessian matrix sums of the left and right child nodes, and λ and γ are the regularization parameters.

The algorithmic principles of XGBoost are: (1) Model Initialization and parameters set. (2) Compute the model's loss function, i.e., objective function. (3) Optimize the objective function to obtain the best splitting node. (4) Generate new tree nodes based on the splitting node and update the model. (5) Repeat steps 2-4 until the stopping criteria are met. Shortcomings of XGBoost are that it requires tuning a large number of parameters, such as tree depth and regularization terms. Therefore, we use grid search to dynamically tune parameters and select the optimal parameters before building the model. The tobacco bacterial wilt disease dataset is divided into a test set and a training set in a 3:7 ratio, and multiple machine learning models are trained and evaluated on the dataset.

2.3.2 Improved target detection algorithm based on RepVGG

Convoluted neural networks (CNNs) are a type of neural network that mimics the human brain and can recognize visual patterns in raw images for object detection tasks. In this study, YOLOX[27] and YOLOv6[28] models from Meituan's Vision Intelligence Department were utilized as the basis for detecting tobacco bacterial wilt, with model improvements made to improve early detection.

(1) Model construction strategy

The YOLO model is typically composed of three components, namely the 'backbone' 'neck' and 'head'[29]. In this study, we aimed to optimize the original YOLOX model by drawing insights from the YOLOv6 model with strong learning performance, as well as the widely-used YOLOv5 model[30]. Since the target model demands higher accuracy and precision in plant disease detection, we focused on directions that could enhance the model's detection accuracy and precision. This involved the selection of training and model construction strategies that could improve the model's accuracy[31].

By analyzing the YOLOX and YOLOv6 algorithms in conjunction with current detection technology research, we improved the YOLOX model and created a new model named Tobacco-AT with insights drawn from the adaptive spatial feature fusion (Adaptively Spatial Feature Fusion, ASFF) method. The mainly improvements to the model include:

1) We used an EfficientRep backbone network based on the RepVGG style, which is highly efficient and can be reparametrized, leading to improved model representation ability and reduced inference latency. To further enhance the model's performance, we replaced the original CSPDarkNet-53 backbone with EfficientRep. As depicted in Figure 8.

2) ASFF is added to the 'neck' part of the network, which enables the network to learn how to spatially filter features at other levels, retaining only useful information for combination (Figure 9). The key idea of ASFF is to adaptively learn the fusion space weight of each scale feature map, which involves two steps: identical scaling and adaptive fusion. Firstly, for a given level of features, other levels of features are adjusted to the same resolution and simply integrated. Then, the best fusion method is learned during training. The vector at the spatial position ($\mathbf{y}^l_{ij}$) after fusion is the weighted fusion of the vectors at the first three feature maps ($\mathbf{x}_{ij}^{1\to l}$, $\mathbf{x}_{ij}^{2\to l}$, $\mathbf{x}_{ij}^{3\to l}$). $\alpha_{ij}^l + \beta_{ij}^l + \gamma_{ij}^l = 1$. The weight coefficients α_{ij}^l, β_{ij}^l, γ_{ij}^l in the formula are learned adaptively by the network, and they are shared among all channels. A 1×1 convolution is used to compute the coefficients in SoftMax so these features can be optimized with standard BP algorithm (Equation (3)).

$$\begin{aligned} \mathbf{y}_{ij}^l &= \alpha_{ij}^l \cdot \mathbf{x}_{ij}^{1\to l} + \beta_{ij}^l \cdot \mathbf{x}_{ij}^{2\to l} + \gamma_{ij}^l \cdot \mathbf{x}_{ij}^{3\to l} \\ \alpha_{ij}^l &= \frac{e^{\lambda_{\alpha ij}^l}}{e^{\lambda_{\alpha ij}^l} + e^{\lambda_{\beta ij}^l} + e^{\lambda_{\gamma ij}^l}} \end{aligned} \tag{3}$$

The coefficients, also known as spatial importance weights, are adaptively learned by the network and shared among all channels. Different levels of features are adaptively fused together at each spatial location. By leveraging the information interaction between different PAN (Path Aggregation Network) feature maps[32], the attention mechanism is used to complete the information fusion and enhancement of the 'neck' part. A simple feature fusion process is illustrated in Figure 9.

3) In addition to the ASFF module in the 'neck' part, we also incorporated the attention mechanism into the Task-aligned predictor of the TOOD (Task-aligned One-stage Object Detection) algorithm to enhance classification and regression features separately[33]. First, the features are compressed by the stem layer (1×1) of the decoupled head, and then the intermediate feature layer is obtained by stacking convolutional layers. Next, the attention mechanism is used to enhance the features of the classification and regression branches separately, effectively decoupling the two tasks. This process is illustrated in Figure 10.

(2) Model training strategy

Due to the limited sample materials, we employed multiple data augmentation strategies and optimized the training approach. Mosaic and MixUp data augmentation techniques were used, although they were turned off in the final 15 epochs to prevent overfitting. We adopted the anchor-free concept, as the anchor-free paradigm has strong generalization ability and simpler decoding logic, which has been widely applied in recent years. And we implemented the SimOTA (Optimal Transport Assignment for Object Detection) label assignment strategy to accelerate the training speed and further improve the detection accuracy[34]. We

also employed the Varifocal Loss function in this study, which is a loss function designed for object detection problems. This function reduces false positive rates while improving object detection accuracy. The method assigns weights to difficult-to-distinguish positive and negative samples, reduces the influence of the difficulty between categories, and enhances the model's detection ability. The formula for Varifocal Loss function is as follows (Equation (4)):

$$VFL(p,q)=\begin{cases}-q(q\log(p)+(1-q)\log(1-p)) & q>0\\ -\alpha p^{\gamma}\log(1-p) & q=0\end{cases} \quad (4)$$

where, p is the predicted IACS (IoU-aware classification score, IoU means Intersection over Union); q is the target score. For a foreground point, the q value of the ground-truth category is set to the IOU (gt_IOU) between the predicted bounding box and the ground-truth. Otherwise, it is 0. For a background point, q is 0 for all target categories.

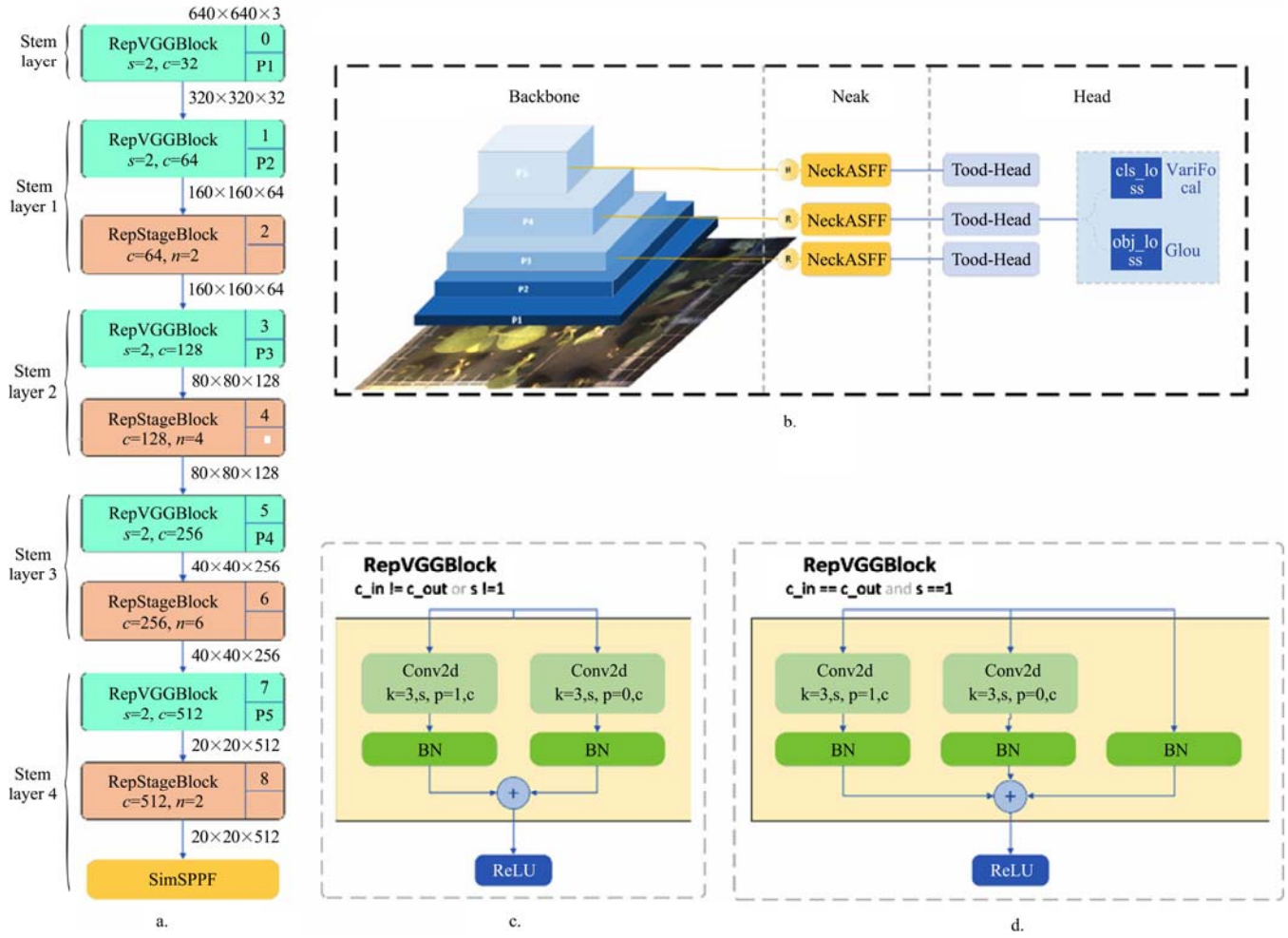

Note: (a) is the backbone network of the network structure, (b) is the overall network structure, (c) and (d) are the RepVGGBlock structure diagrams.

Figure 8 Network structure diagram

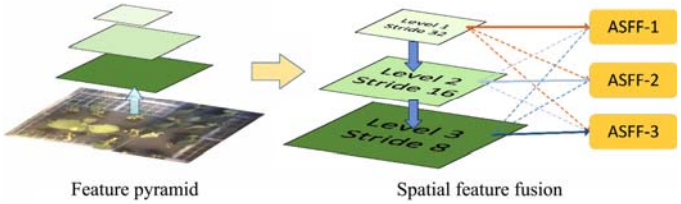

Note: Each layer of the 'feature pyramid' is adjusted to the same scale, and spatial fusion is performed according to the weight.

Figure 9 ASFF information fusion

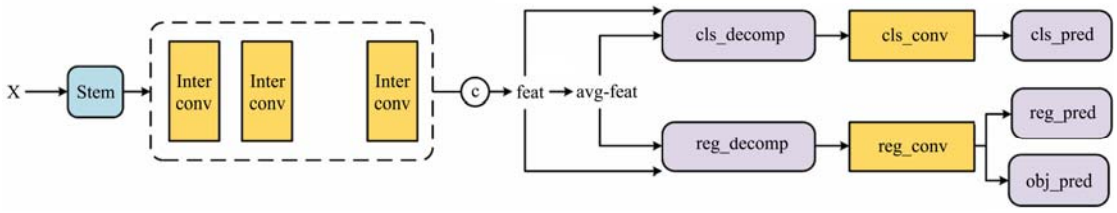

Figure 10 Attention mechanism

2.3.3 Evaluating indicator

Accuracy is a commonly used evaluation index that is defined as the number of correct predictions divided by the total number of samples (Equation (5)). The higher the accuracy, the better the

classifier performs. Precision is defined as the proportion of positive examples that are correctly identified by the classifier (Equation (6)).

$$ACC = \frac{TP + TN}{TP + TN + FP + FN} \tag{5}$$

$$P = \frac{TP}{TP + FP} \tag{6}$$

True Positive (TP): The number of positive samples that are correctly predicted as positive by the classifier. True Negative (TN): The number of negative samples that are correctly predicted as negative by the classifier. False Positive (FP): The number of negative samples that are incorrectly predicted as positive by the classifier. False Negative (FN): The number of positive samples that are incorrectly predicted as negative by the classifier.

We introduced the commonly used evaluation criterion mAP (mean Average Precision). The AP (Average Precision) value is the area under the PR (Precision-Recall Curve) curve enclosed by the coordinate axis. P is Precision and R is Recall (Equation (7)). In object detection tasks, the definitions of TP and FP are different. Simply put, the object detector predicts multiple boxes. The number of successful matches with ground truth is TP, and the rest are FP.

$$Recall = \frac{TP}{TP + FN} \tag{7}$$

These modules, comprising the mAP (mean Average Precision) and its variants, play a pivotal role in objectively evaluating the efficacy of object detection models, facilitating the assessment of their ability to accurately detect and localize objects under different evaluation criteria.

1) mAP@[.5:.95] (mean Average Precision over IoU range [.5:.95]): In contrast to mAP@0.75, this metric offers a comprehensive evaluation by considering a range of IoU thresholds from 0.5 to 0.95, with a defined interval. This range encompasses various levels of bounding box overlap, allowing a more nuanced assessment of a model's performance across diverse object sizes and shapes.

2) mAP@0.75 (mean Average Precision at IoU (Intersection over Union) 0.75): This specific variant of mAP focuses on assessing a model's ability to precisely localize objects within images. It evaluates the average precision at a predefined intersection over union (IoU) threshold of 0.75. A higher IoU threshold emphasizes stricter overlap criteria for bounding boxes, which is particularly relevant when precise localization is of paramount importance.

3 Results and analysis

3.1 Hyperspectral data modeling and evaluation

For ease of processing, we numbered the 224 bands of hyperspectral data from 1 to 224, as detailed in Appendix 1. We used the partitioned tobacco bacterial wilt hyperspectral dataset for testing and evaluation. The dataset is at the leaf scale and covers the entire disease process of the second batch of materials. It contains a total of 275 data points, with 75 data points in the test set. We used three preprocessing methods: first-order derivative (da), second-order derivative (dda), and Log function (log), and combined them with random forest (RF), logistic regression (logistics), and support vector machine (SVM) for pre-experimentation on the dataset. As shown in Figure 15, the classification performance of the first-order derivative (da) combined with these four classifiers is the best. Therefore, the first-order derivative (da) is the optimal preprocessing method. The visualization results are shown in Figure 11.

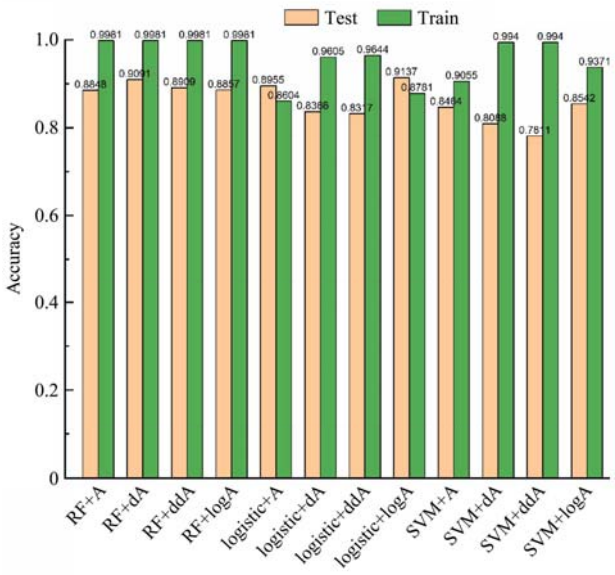

Figure 11 Hyperspectral data preprocessing results

We used the partitioned tobacco bacterial wilt hyperspectral preprocessed dataset for testing. The test set contains 75 data points. We used XGBoost, LightGBM, and SVM classification algorithms to model and output results, and plotted the results. As shown in Figure 12.

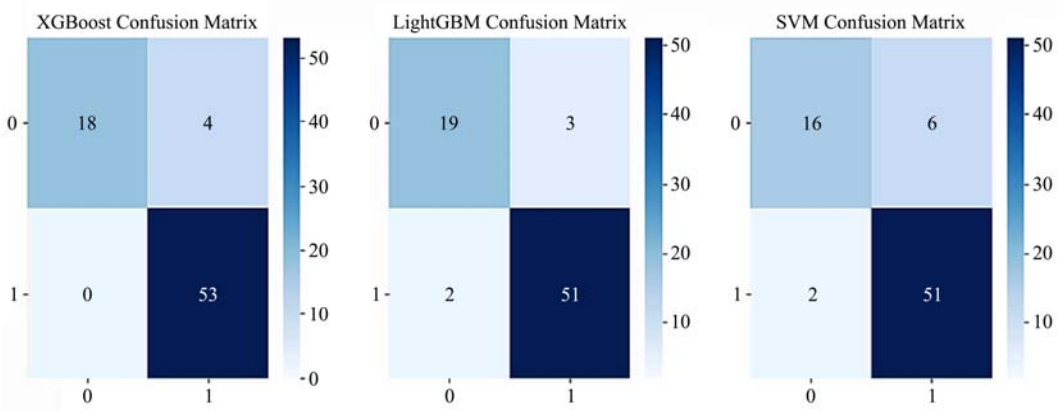

Figure 12 Classifier performance comparison

The classification accuracy and precision of the three classifiers is shown in Table 1. #Based on the requirements of the disease detection task, we chose the XGBoost model with the highest Precision and then built the model.

Table 1 Classification model evaluation results

Classifier	Precision	Accuracy
SVM	89.47%	89.33%
XGBoost	92.98%	94.67%
LightGBM	94.44%	93.33%

For testing, we used the labeled average reflectance dataset for model training and verification. We used a feature selection algorithm to obtain the characteristic bands of tobacco bacterial wilt susceptible leaves. The contribution rate of each band to the discriminant results is shown in Figure 13. Three bands with the largest contribution rate, 566.741 nm, 706.026 nm, 815.849 nm, were selected.

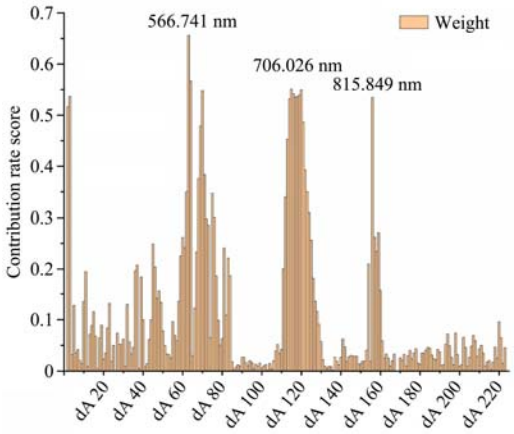

Figure 13 Classifier performance comparison results

We divide new data according to the characteristic bands of 566.741 nm, 706.026 nm, 815.849 nm and combine support vector machine (SVM), Extreme Gradient Boosting (XGBoost), Logistic Regression (Logistic) and stepwise regression (RS) to build the model. The accuracy of the model using all features is represented as 'dA_{all}', while the accuracy of the model using feature bands is represented as 'dA_x'. The results are shown in Table 2, and the XGBoost model achieved the best accuracy of 92.20%.

Table 2 Characteristic band model validation results table

Model	dA_{all}	dA_x
SVM	93.00%	88.00%
XGBoost	99.04%	92.20%
Logistic	95.12%	83.27%
SR	95.00%	81.00%

3.2 Evaluation of proposed Tobacco-AT model

The dataset used in this study was prepared by organizing and preprocessing daily visible light images. For annotation, the COCO dataset format was employed, with each type of annotation corresponding to a JSON file containing comprehensive information about the images, categories, and specific annotations. The created dataset was randomly divided into training set, validation set and test set with a ratio of 6:2:2. Additionally, a periodic evaluation testing set was created based on the time interval after inoculation. MMYOLO, an open-source toolbox based on the YOLO series algorithm and PyTorch/MMDetection, was used for this experiment. MMYOLO is part of the OpenMMLab project (https://github.com/open-mmlab/mmyolo). Before training, we configured the basic training parameters. The input image size was set to 640×640, the number of epoch was 100, and the batch size was set to 8. We recorded every two epochs from 20-90 and all the last ten epochs. The model saved the optimal weight file. Training was performed using an NVIDIA Tesla M40 graphics card. We selected the widely used YOLOv5 and the recently released YOLOv6 and YOLOv8 as comparison models.

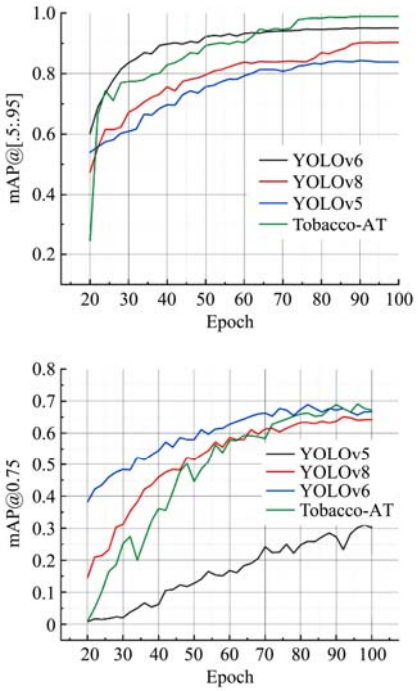

Figure 14 Model evaluation results

The evaluation index used in the COCO dataset includes the IOU threshold, with AP50 representing the AP at an IOU threshold greater than 0.5 and AP75 representing the same at an IOU threshold greater than 0.75. The Tobacco-AT model, which uses the EfficientRep backbone and Varifocal Loss function, achieved faster convergence and a map_50 evaluation standard of 95.30% at the 22nd epoch. As shown in Figure 14. Furthermore, the map_50 values of the final ten epochs reached 99.00%, and the Tobacco-AT model outperformed other models in the map_75 standard, achieving 96.70%. As shown in Table 3.

Table 3 Summary of optimal model results

Model	mAP@ [.5:.95]	mAP@0.75
YOLOv5	83.80%	30.20%
YOLOv8	90.30%	64.20%
YOLOv6	95.10%	66.70%
Tobacco-AT	98.90%	67.20%

To compare the performance of the YOLOv6 and Tobacco-AT models on the test set, their prediction results were compared. Both models exhibited good overall prediction performance, but the Tobacco-AT model with ASFF information fusion performed better in detecting diseased leaves, especially for small and edge leaves (Figure 15a). The occlusion of objects has always been a challenging problem in target detection. In the case of mutual occlusion of leaves, the Tobacco-AT model can accurately identify two diseased leaves (Figure 15b). This is because the model can leverage the ASFF information fusion mechanism to integrate multi-level features, which helps to capture more contextual information and improve the model's ability to recognize partially occluded objects. Additionally, the Varifocal Loss function used in the Tobacco-AT model can assign different weights to different parts of the object, which helps the model to focus more on the visible parts of the occluded object and reduce the interference caused by the occlusion.

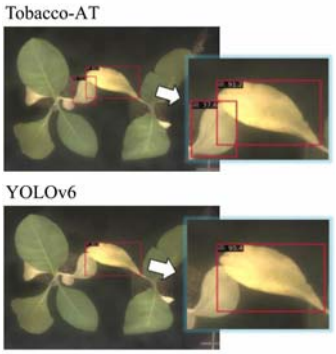

a. Show the detection of occluded leaves

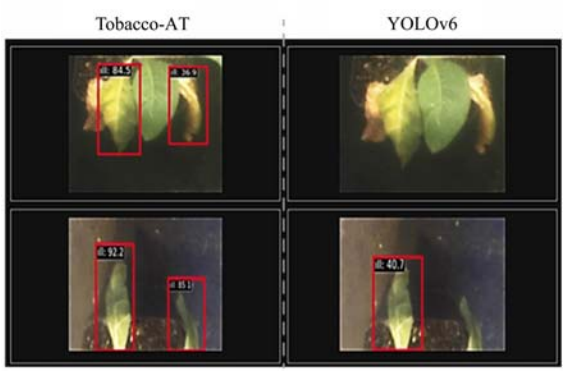

b. Shows the detection of small objects at the edge

Figure 15 Comparison of model prediction results for more difficult tasks

3.3 Comparison of hyperspectral and visible light model effects

Because tobacco plants are susceptible to tobacco bacterial wilt throughout their growth period, and the disease progresses from the roots upward, with varying durations of disease onset, the accuracy of early detection and continuous detection throughout the disease cycle are particularly important for the model evaluation.

We created a new test set based on the number of days after inoculation and evaluated the two models accordingly. We compared the improved visible light model (Tobacco-AT) with the high-spectral feature band model (XGBoost-Hypespectral) and found that in the early stages of bacterial wilt infection (days 1-2 after onset), which is difficult to observe by the naked eye, the high-spectral model significantly outperformed the visible light model. The high-spectral model achieved an accuracy of 69.57% on the first day of detection, while the improved Tobacco-AT model had an accuracy of 54.66%. In the middle and late stage of the onset of bacterial wilt, that is, when the symptoms are more obvious (after the third day), the accuracy of the visible light model gradually surpassed that of the hyperspectral model, and the two models had the same effect in the later stage (Figure 16). Table 4 shows the accuracy of hyperspectral and visible light model for bacterial wilt detecting day by day.

Table 4 Comparison of hyperspectral and visible light results day by day

Days	Hyperspectral	Visible light
1	69.57%	54.66%
2	70.83%	66.00%
3	86.36%	85.00%
4	94.66%	93.33%
5	100%	100%
6	100%	100%
7	100%	100%

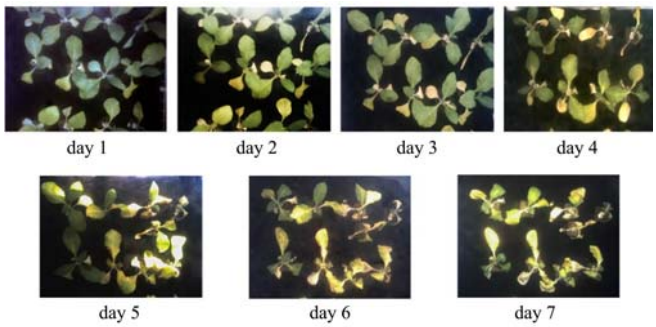

Note: The above figures show the changes in tobacco plants infected with bacterial wilt disease over a week, while the figures below compare the accuracy of the two detection methods throughout the entire disease cycle.

Figure 16 Comprehensive comparison of disease cycle

4 Discussion

The primary focus of this study was to investigate early detection methods for tobacco bacterial wilt disease in indoor tobacco plants. Phenotyping methods were employed to establish an early detection model for the disease and identify the hyperspectral reflection bands that exhibit sensitivity to tobacco bacterial wilt. Hyperspectral imaging technology, while capable of providing detailed information, poses challenges in terms of data processing and equipment cost. To address these concerns, the feasibility of using a multispectral camera for data collection was considered to reduce costs and simplify the process. However, this approach necessitates robustness in both the model and the selection of feature bands. It is important to note that in this study, data collection was solely conducted using a hyperspectral camera without further expansion. For example, Cen Yi et al. have developed a portable hyperspectral acquisition device for collecting tomato bacterial wilt leaf data. This device can be applied under various conditions and is not restricted by natural light limitations[35]. Kamlesh Golhani, Siva K. Balasundram summarized the method of applying neural network to spectral data, but the amount of data and the robustness of the model still need to be enhanced, which is also very inspiring to our work[36].

Through the analysis of the data results of this experiment, we used a hyperspectral camera to collect data on the plants at the earliest stage of disease occurrence, and then used the model we established to identify the disease. The accuracy achieved is higher than that of the visible light method. The visible light model is difficult to capture changes in plants at the earliest stage but can keenly identify susceptible plants at a later stage. At the same time, the processing flow and computational requirements of hyperspectral methods are far greater than those of visible light methods. We will also continue to explore the advantages of the two methods to combine the advantages of the two sensors. How to align the data and whether it can be aligned at the pixel level is still a challenge. The role played by attention mechanisms has also led to our interest in multimodal data approaches.

5 Conclusions

This study introduces two non-destructive methods for early detection of tobacco bacterial wilt disease in indoor plants. These approaches offer rapid and non-destructive detection, surpassing conventional techniques. The XGBoost-Hyperspectral full-band model achieves an impressive accuracy of 99.04% on the comprehensive testing set, with 69.57% accuracy attained on the first day of the disease cycle. Furthermore, the feature band model based on the XGBoost algorithm demonstrates high

detection accuracy of 92.20%, utilizing only a select few specific bands.

For visible light detection, deep learning methods exhibit exceptional capability in capturing the "wilting" feature from visible light images, effectively overcoming the challenge faced by traditional algorithms in precisely identifying early disease symptoms. The enhanced Tobacco-AT model showcases remarkable improvements, achieving an accuracy of 98.90% in the test dataset. While early detection accuracy is comparatively lower, it reaches 85.00% on the third day, equivalent to the performance of the hyperspectral method. These results emphasize the effectiveness and timeliness of both methods for early detection of tobacco bacterial wilt disease.

Author contributions

X.Z., Y. L., J. L. and Z. P. performed the experiments. X.Z. analyzed the data and wrote the original draft. Y. L., L. Z. and W. Y. funding support and revised the manuscript. P. S. designed the research, supervised the project and revised the manuscript. All authors contributed to the article and approved the submitted version.

Acknowledgements

This work was supported by Pests and Diseases Green Prevention and Control Major Special Project (Grant no. 110202101045, LS-05), the National Key R&D Program of China (2022YFD2002304), the Major Project of Hubei Hongshan Laboratory (2022hszd004), Fundamental Research Funds for the Central Universities (2662022JC006), National Natural Science Foundation of China (U21A20205) and HZAU-AGIS Cooperation Fund (SZYJY2022014).

Conflict of interest

The authors declare that the research was conducted in the absence of any commercial or financial relationships that could be construed as a potential conflict of interest.

Data availability

The datasets generated and analyzed during the current study are available at https://github.com/I-am-zxf/tobacco-bacterial-wilt.

[References]

[1] André, d. S. X., Fraleon, d. A. J. C., Gonçalves, d. M. A., M, R. G., M, T. D., Reis, d. R. R., Sylvain, M., Poliane, A.-Z. Characterization of CRISPR-Cas systems in the Ralstonia solanacearum species complex. Molecular plant Pathology, 2019, 20(2). doi: 10.1111/mpp.12750

[2] Hayward, A. C. Biology and Epidemiology of Bacterial Wilt Caused by Pseudomonas Solanacearum. Annual Review of Phytopathology, 1991, 29(1). doi: 10.1146/annurev.phyto.29.1.65

[3] Chávez, P., Yarlequé, C., Loayza, H., Mares, V., Hancco, P., Priou, S., Márquez, M. d. P., Posadas, A., Zorogastúa, P., Flexas, J. Detection of bacterial wilt infection caused by Ralstonia solanacearum in potato (Solanum tuberosum L.) through multifractal analysis applied to remotely sensed data. Precision Agriculture, 2012, 13, 236–255. doi: 10.1007/s11119-011-9242-5

[4] Xie, C., Shao, Y., Li, X., He, Y., Detection of early blight and late blight diseases on tomato leaves using hyperspectral imaging. Scientific reports 2015, 5(1): 16564. doi: 10.1038/srep16564

[5] Mahlein, A. K., Kuska, M. T., Behmann, J., Polder, G., Walter, A., Hyperspectral Sensors and Imaging Technologies in Phytopathology: State of the Art. Annu Rev Phytopathol 2018, 56, 535–558. doi: 10.1146/annurev-phyto-080417-050100

[6] Yang, W., Duan, L., Chen, G., Xiong, L., Liu, Q. Plant phenomics and high-throughput phenotyping: accelerating rice functional genomics using multidisciplinary technologies. Current Opinion in Plant Biology, 2013, 16(2): 180–187. doi: 10.1016/j.pbi.2013.03.005

[7] Aaron, P., Sara, P., Albert, C., Corely, H. C., Jose, D. G. I., Changying, L. High throughput phenotyping of tomato spot wilt disease in peanuts using unmanned aerial systems and multispectral imaging. IEEE Instrumentation & Measurement Magazine, 2017, 20(3). doi: 10.1109/MIM.2017.7951684

[8] Ali, H., Lali, M. I., Nawaz, M. Z., Sharif, M., Saleem, B. A. Symptom based automated detection of citrus diseases using color histogram and textural descriptors. Computers & Electronics in Agriculture, 2017, 138(C): 92–104. doi: 10.1016/j.compag.2017.04.008

[9] Arnal, B. J. G. An Automatic Method to Detect and Measure Leaf Disease Symptoms Using Digital Image Processing. Plant disease, 2014, 98(12). doi: 10.1094/PDIS-03-14-0290-RE

[10] Zhang, M., Chen, T., Gu, X., Chen, D., Wang, C., Wu, W., Zhu, Q., Zhao, C. Hyperspectral remote sensing for tobacco quality estimation, yield prediction, and stress detection: A review of applications and methods. Front Plant Sci, 2023, 14, 1073346. doi: 10.3389/fpls.2023.1073346

[11] Gu, Q., Sheng, L., Zhang, T., Lu, Y., Zhang, Z., Zheng, K., Hu, H., Zhou, H. Early detection of tomato spotted wilt virus infection in tobacco using the hyperspectral imaging technique and machine learning algorithms. Computers and Electronics in Agriculture, 2019, 167, 105066. doi: 10.1016/j.compag.2019.105066

[12] Yusuf, B. L., He, Y. Application of hyperspectral imaging sensor to differentiate between the moisture and reflectance of healthy and infected tobacco leaves. Afr. J. Agric. Res, 2011, 6(29): 6267–6280. doi: 10.5897/AJAR11.1281

[13] Terentev, A., Dolzhenko, V., Fedotov, A., Eremenko, D.. Current State of Hyperspectral Remote Sensing for Early Plant Disease Detection: A Review. Sensors (Basel), 2022, 22(3): 757. doi: 10.3390/s22030757

[14] Hongyan, Z., Bingquan, C., Chu, Z., Fei, L., Linjun, J.,Yong, H. Hyperspectral Imaging for Presymptomatic Detection of Tobacco Disease with Successive Projections Algorithm and Machine-learning Classifiers. Scientific reports, 2017, 7(1). doi: 10.1038/s41598-017-04501-2

[15] Camargo, Smith, J S. An image-processing based algorithm to automatically identify plant disease visual symptoms. Biosyst Eng, 2009. doi: 10.1016/j.biosystemseng.2008.09.030

[16] Shi, Y., Huang, W., Luo, J., Huang, L., Zhou, X. Detection and discrimination of pests and diseases in winter wheat based on spectral indices and kernel discriminant analysis. Computers & Electronics in Agriculture, 2017, 141, 171–180. doi: 10.1016/j.compag.2017.07.019

[17] Wang, D., Tan, X. Unsupervised Feature Learning with C-SVDDNet. 2014. doi: 10.1016/j.patcog.2016.06.001

[18] Phadikar, S., Sil, J., Das, A. K. Feature selection by attribute clustering of infected rice plant images. International Journal of Machine Intelligence 2011, 3(2). doi: 10.9735/0975-2927.3.2.74-88

[19] Sujatha, R., Chatterjee, J. M., Jhanjhi, N., Brohi, S. N. Performance of deep learning vs machine learning in plant leaf disease detection. Microprocessors and Microsystems, 2021, 80, 103615. doi: 10.1016/j.micpro.2020.103615

[20] A, G. R., B, S. S., B, J. M. M., C, W. S. L., A, J. R., B, R. E. Comparison of two aerial imaging platforms for identification of Huanglongbing-infected citrus trees. Computers and Electronics in Agriculture, 2013, 91(1): 106-115. doi: 10.1016/j.compag.2012.12.002

[21] Liang, Q., Xiang, S., Hu, Y., Coppola, G., Zhang, D., Sun, W. PD 2 SE-Net: Computer-assisted plant disease diagnosis and severity estimation network. Computers and Electronics in Agriculture, 2019, 157, 518–529. doi:10.1016/j.compag.2019.01.034

[22] Zeng, W., Li, M. Crop leaf disease recognition based on Self-Attention convolutional neural network. Computers and Electronics in Agriculture 2020, 172(C). doi: 10.1016/j.compag.2020.105341

[23] Afework, Y. K., Debelee, T. G. Detection of bacterial wilt on enset crop using deep learning approach. International Journal of Engineering Research in Africa, 2020, 51, 131–146. doi: 10.4028/www.scientific.net/JERA.51.131

[24] Huang, C., Zhang, Z., Zhang, X., Jiang, L., Hua, X., Ye, J., Yang, W., Song, P., Zhu, L. A Novel Intelligent System for Dynamic Observation of Cotton Verticillium Wilt. Plant Phenomics, 2023, 5, 0013. doi: 10.34133/plantphenomics.0013

[25] Sutton, S. Measurement of cell concentration in suspension by optical density. Microbiology, 2006, 585, 210–8336.

[26] Chen, T., Guestrin, C. In Xgboost: A scalable tree boosting system, Proceedings of the 22nd acm sigkdd international conference on knowledge discovery and data mining, 2016, pp785–794.

[27] Ge, Z., Liu, S., Wang, F., Li, Z., Sun, J. Yolox: Exceeding yolo series in

2021. arXiv preprint arXiv:2107.08430 2021. doi: 10.48550/arXiv.2107.08430

[28] Li, C., Li, L., Jiang, H., Weng, K., Geng, Y., Li, L., Ke, Z., Li, Q., Cheng, M., Nie, W. YOLOv6: A single-stage object detection framework for industrial applications. arXiv preprint arXiv:2209.02976, 2022. doi: DOI:10.48550/arXiv.2209.02976

[29] Redmon, J., Divvala, S., Girshick, R., Farhadi, A. In You only look once: Unified, real-time object detection, Proceedings of the IEEE conference on computer vision and pattern recognition, 2016, pp779–788.

[30] Zhu, X., Lyu, S., Wang, X.,Zhao, Q. TPH-YOLOv5: Improved YOLOv5 Based on Transformer Prediction Head for Object Detection on Drone-captured Scenarios, 2021. doi: 10.48550/arXiv.2108.11539

[31] Saleem, M. H., Potgieter, J., Mahmood Arif, K. Plant disease detection and classification by deep learning. Plants (Basel), 2019, 8(11): 468. doi: 10.3390/plants8110468

[32] Liu, S., Qi, L., Qin, H., Shi, J., Jia, J. Path Aggregation Network for Instance Segmentation. 2018 IEEE/CVF Conference on Computer Vision and Pattern Recognition (CVPR), 2018. doi: 10.1109/CVPR.2018.00913

[33] Feng, C., Zhong, Y., Gao, Y., Scott, M. R., Huang, W. In Tood: Task-aligned one-stage object detection, 2021 IEEE/CVF International Conference on Computer Vision (ICCV). IEEE Computer Society, 2021, pp3490–3499.

[34] Ge, Z., Liu, S., Li, Z., Yoshie, O., Sun, J. In Ota: Optimal transport assignment for object detection, Proceedings of the IEEE/CVF Conference on Computer Vision and Pattern Recognition, 2021, pp303–312.

[35] Cen, Y., Huang, Y., Hu, S., Zhang, L., Zhang, J. Early detection of bacterial wilt in tomato with portable hyperspectral spectrometer. Remote Sensing, 2022, 14(12): 2882. doi: 10.3390/rs14122882

[36] Golhani, K., Balasundram, S. K., Vadamalai, G., Pradhan, B. A review of neural networks in plant disease detection using hyperspectral data. Information Processing in Agriculture 2018, 5(3): 354–371. doi: 10.1016/j.inpa.2018.05.002